Search for isovector giant monopole resonances via the ^{124}Sn(^{3}He,tn) reaction

R. G. T. Zegers, S. Brandenburg, M. N. Harakeh, and S. Y. van der Werf
Kernfysisch Versneller Instituut, Zernikelaan 25, 9747 AA Groningen, The Netherlands

J. Jänecke, T. O'Donnell, D. A. Roberts, and S. Shaheen*
Department of Physics, University of Michigan, Ann Arbor, Michigan 48109

G. P. A. Berg, C. C. Foster, T. Rinckel, and E. J. Stephenson
Indiana University Cyclotron Facility, Bloomington, Indiana 47405
(Received 6 October 1999; published 30 March 2000)

The (^{3}He,t) reaction on ^{124}Sn at $E(^3\mathrm{He})=199$ MeV and the subsequent decay by neutron emission at backward angles were studied in an attempt to distinguish isovector monopole strength (spin-flip and non-spin-flip) at excitation energies above 25 MeV from the nonresonant continuum. The present approach is based on the assumption that a large fraction of the contributions to the continuum result from quasifree processes and breakup-pickup processes which leave the nucleus in low-lying excited states below the threshold for neutron emission. It was found, however, that even at high ''apparent'' excitation energies (above 30 MeV) the branching ratio for decay by neutrons was as high as $\sim$50%, indicating that a large part of the nonresonant continuum may not be due to quasifree processes involving valence neutrons only. No evidence for monopole strength at high excitation energies was found, although the experiment had sufficient sensitivity and accuracy to detect isovector monopole strength based on theoretical predictions calculated in the framework of normal-mode collective excitations and the distorted-wave Born approximation.

PACS number(s): 24.30.Cz, 25.55.Kr, 27.60.+j

I. INTRODUCTION

Isovector giant monopole resonance (IVGMR, $\Delta L=0$, $\Delta S=0$, $\Delta T=1$) can be described macroscopically by compressional, out-of-phase, breathing oscillations of protons and neutrons in the nucleus. Its spin-flip partner, isovector spin-flip monopole resonance (IVSMR, $\Delta L=0$, $\Delta S=1$, $\Delta T=1$) is more difficult to describe in this picture. In a microscopic approach, both resonances can be described as coherent superpositions of $2\hbar\omega$ one-particle–one-hole (1p-1h) excitations, with a change in principal quantum number by 1 and no change in orbital angular momentum.

Isovector monopole resonances have been a subject of interest for several decades. They are of intrinsic interest since they represent fundamental modes of collective nuclear excitations and play an important role in understanding nuclear-structure and Coulomb effects. In particular, IVGMR mediates isospin mixing via the long-range monopole term of the Coulomb interaction between IVGMR and the isobaric analog state (IAS). Monopole resonances are, however, very difficult to study experimentally. Evidence for IVGMR was found [1–3] in the (π^-,π^0) reaction ($\Delta T_z=+1$) on various targets, but for the (π^+,π^0) reaction ($\Delta T_z=-1$) the data are less convincing. Recently, strong indications for IVGMR in ^{60}Co was found by Nakayama *et al.* [4] using the ^{60}Ni(^{7}Li,^{7}Be) reaction. Structure at high excitation energies, which might possibly be associated with IVGMR, has been reported in the ^{90}Zr(n,p) reaction [5] and in the (^{13}C,^{13}N) reaction [6–8]. Conclusions with respect to multipolarity, however, could not be drawn from the observed shape of the spectra at high excitation energies and the derived strength. In the (^{13}C,^{13}N) reaction [7], neutron decay was also studied in coincidence with the scattered ejectiles. However, the large anisotropy observed for neutron decay is not compatible with the excitation of IVGMR. Indications for IVSMR were first found in the ^{90}Zr(^{3}He,t) reaction at projectile energies of 600 and 900 MeV [9,10]. Also, in the (p,n) reaction at 795 MeV on ^{90}Zr and Pb, strength was observed that is consistent with collective states of $J^\pi=1^+$ [11].

It should be noted that neutron decay in coincidence with charge-exchange reactions has been used previously to investigate damping mechanisms of charge-exchange giant resonances including isobaric analog states [12,13,7].

In all the experimental work related to IVGMR and IVSMR mentioned above, the interpretation is seriously complicated by the presence of a large, nonresonant, continuum background due to the quasifree knock-on charge-exchange process. This process is a charge-exchange reaction between the projectile and one of the target neutrons in (p,n)-type reactions or one of the protons in (n,p)-type reactions. In addition, processes usually referred to as pickup-breakup and breakup-pickup processes contribute to this continuum in the case of charge-exchange reactions initiated with nuclear projectiles. This continuum, in combination with the large widths of the resonances under study, hampers the interpretation of the spectra. In the present (^{3}He,t) reaction the main contribution of the continuum background comes from the quasifree knock-on charge-exchange process, because the breakup-pickup process peaks at a much higher ''apparent'' excitation energy [14–16]; see also Sec. III. Furthermore, in case of the (^{3}He,t) reaction the pickup-breakup process hardly contributes because it results in a

*Permanent address: King Abdulaziz University, Jeddah, Saudi Arabia.

strongly stable intermediate channel, the α particle. A phenomenological description, as first used by Erell *et al.* [1] for the π-charge-exchange reaction, to describe the quasifree knock-on charge-exchange process and its dependence on the ''apparent'' excitation energy was subsequently used also to describe the continuum background in the $(^3\mathrm{He},t)$ reaction at the present bombarding energy [17].

Since the early 1970s various theoretical approaches have been developed to describe IVGMR and IVSMR. Estimates for the transition matrix elements of IVGMR were given by Auerbach in 1972 [18]. In 1975, calculations in a hydrodynamical framework were performed by Auerbach and Yeverechyahu [19]. In anticipation of the experimental results from the π-charge-exchange experiments, microscopic calculations for IVGMR were performed [20–22]. For IVSMR, hydrodynamical calculations are difficult because of the spin degree of freedom. Auerbach and Klein also performed calculations for IVSMR in a Hartree-Fock (HF), random-phase approximation (RPA) framework [23], concluding that the strength distributions for IVGMR and IVSMR are similar. The relative contributions from the two resonances to the monopole cross section are determined by the energy dependence of the effective nucleon-nucleon (NN) interaction and the Q-value dependence of the reaction mechanism [24,25]. At high incoming energies of $E \geqslant 100$ MeV/nucleon isovector non-spin-flip transitions mediated through the V_τ component of the effective force are strongly quenched while contributions from spin-flip transitions (mediated through the $V_{\sigma\tau}$ and $V_{T\tau}$ components of the effective force) dominate. The situation is reversed at energies lower than 50 MeV/nucleon. Furthermore, at energies below 50 MeV/nucleon the cross sections of IVSMR and IVGMR are expected to decrease strongly as a function of excitation energy because of the increasing momentum mismatch. This is confirmed by the distorted-wave Born approximation (DWBA). The experiment described here was performed at 66 MeV/nucleon, where the expected cross section for IVGMR reaches a maximum, although it is still considerably lower than that expected for IVSMR (see below).

We used the $(^3\mathrm{He},t)$ reaction in an attempt to find the $\Delta T_z = -1$ components of IVGMR and IVSMR. In the $(^3\mathrm{He},t)$ reaction, the charge-exchange and breakup-pickup processes all result in a proton particle in the continuum and a neutron-hole state, and thus result in (semi)direct proton emission. Neutron emission from populated giant resonances and/or deeply bound neutron-hole states can only be statistical as discussed further below. Therefore, the experiment was designed to look at statistical neutron decay with high efficiency. Note that for (n,p)-like reactions the situation is reversed; i.e., a neutron particle in the continuum and a proton-hole state are created, thus resulting in (semi)direct neutron emission.

In order to reduce the continuum at higher excitation energies, a coincidence between tritons at forward angles and neutrons emitted at backward angles was required. The tritons produced in quasifree and breakup-pickup reactions are expected in coincidence with high-energy, forward-peaked protons. These processes leave the final nucleus in low-lying excited neutron-hole states since the ^{3}He particle is expected to probe the surface of the nucleus strongly [26]. Emission of neutrons is therefore unlikely because of the relatively high neutron-separation energy ($S_n = 5.95$ MeV). The pickup-breakup process should not contribute to the continuum in the $(^3\mathrm{He},t)$ reaction since by picking up a neutron a relatively stable ^{4}He particle would be created.

IVGMR and IVSMR can decay in various ways. Statistical decay is most likely to happen through emission of neutrons and γ rays since the Coulomb barrier strongly inhibits statistical proton emission in heavy nuclei. Direct decay, however, is most likely to occur by emission of protons. This decay mode can be quantitatively understood because IVGMR and IVSMR can each microscopically be described as a coherent superposition of 1p-1h states. Semidirect decay can also occur before full equilibrium is reached. Independent of the decay mode, decay from IVGMR and IVSMR must be isotropic because of their monopole character. Thus, by measuring coincidences between tritons around $0°$ (the monopole cross sections peak strongly at forward angles) and neutrons at backward angles these (and possibly other) resonances should be separable from the quasifree and breakup-pickup processes.

II. EXPERIMENTAL SETUP

The experiment was carried out at the Indiana University Cyclotron Facility (IUCF). A 199-MeV $^3\mathrm{He}^{2+}$ beam was accelerated in the dual-cyclotron setup and transported to the K600 spectrometer. The K600 spectrometer consists of a hexapole, a quadrupole, and two dipole magnets. In addition, two dipole pole-face current windings are present which allow ''hardware'' aberration corrections. The focal-plane detection system consists of a wire chamber array backed by two scintillator detectors. The latter are used to provide particle identification, the event trigger, and also the stop signal for the time-of-flight measurement with respect to the rf frequency of the cyclotron. The wire-chamber array consists of two vertical-drift chambers (VDC's) and two horizontal-drift chambers (HDC's), enabling horizontal and vertical positions and angle measurements at the focal plane. A more detailed discussion of the K600 spectrometer and its components can be found in various IUCF annual reports [27–29].

Measurements with a multihole collimator defining the spectrometer aperture at $20°$ were performed using elastically scattered $^3\mathrm{He}^{2+}$ particles to determine the ray-trace parameters necessary to calculate the scattering angles for the particles detected in the focal plane. At the higher magnetic field needed to bend the tritons (factor of 2), saturation effects resulted in distortions in the optics which could only partly be corrected for. Consequently, the ray-trace parameters for the vertical component of the scattering angle could not be used, leaving only the horizontal component of the scattering angle for the analysis.

Details of experimental techniques used to measure triton spectra near $0°$ have been described before [13,17,30,31] and will only be briefly reviewed here. In the experiment an angle-defining circular aperture with a diameter of 70 mrad was used. The spectrometer was set at -10 mrad; i.e., the beam enters the spectrometer off center, closer to the con-

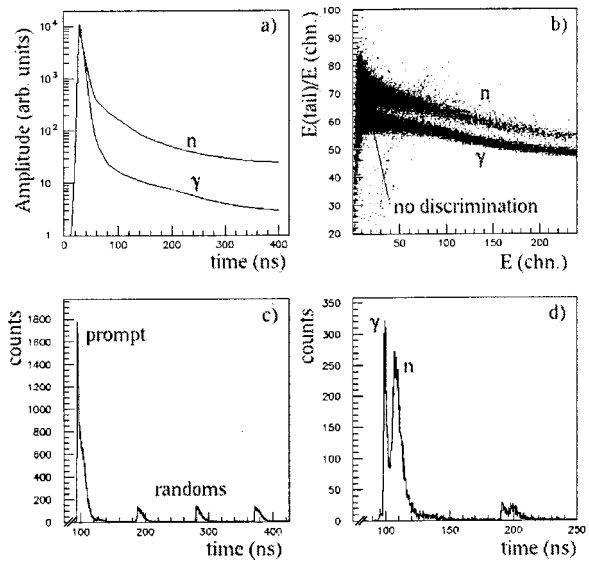

FIG. 1. Procedure for neutron-γ discrimination. (a) Pulse shapes for the NE213 scintillating material. (b) Scatterplot for events with integrated tail of pulse (E_{tail}) divided by integrated total pulse (E) vs E. (c) Time structure of prompt and random coincidences, and likewise (d) for particles with low E.

cave edge of the dipole. The beam was stopped in an electrically insulated graphite beam dump which was placed inside the first dipole magnet of the spectrometer. The beam current ($\sim 1e$ nA) was read out for absolute cross-section determination.

To cover a sufficiently large range of excitation energies, measurements at two different field settings were performed, each covering approximately 30 MeV in excitation energy (for the K600, $\Delta E/E \approx 16\%$) and thus overlapping by 10 MeV. The target was enriched (97.2%) ^{124}Sn of 7.7 mg/cm^2 thickness.

The reaction ^{124}Sn(^{3}He,t)^{124}Sb was chosen because it had been investigated previously [17] at $E(^3\mathrm{He}) = 200$ MeV, and cross sections for states and resonances are known for $E_x < 26$ MeV. Furthermore, the branching ratio for neutron decay from the IAS in ^{123}Sb is estimated at 91.1 ± 5.0 % [32]. This IAS can therefore be used as a convenient calibration for the expected yield of IVGMR and IVSMR. Compared to the neutron decay from the IAS in ^{120}Sb which was studied earlier [13] with a maximum neutron energy of 3.2 MeV (average energy ~ 850 keV), the corresponding energy for the decay from ^{124}Sb is almost a factor of 2 higher with some increase in the average decay energy. This should simplify the detection of decay neutrons.

Neutrons were detected in four NE213 and four NE230 liquid scintillators (diameter 5 cm$\times$5 cm), which were chosen because of their good neutron-γ pulse-shape discrimination (PSD) properties. The detectors were mounted at backward angles, at ~ 8 cm from the target. The distance was kept small in order to cover a relatively large solid angle (13% of 4π). The procedure for neutron-γ discrimination by means of time of flight (TOF) and PSD is illustrated in Fig. 1. Because of the short distance neutron-γ separation by means of TOF, measurement was possible only for the slowest neutrons. Excellent discrimination was, however, achieved by combining PSD for all neutron energies [see Figs. 1(a) and 1(b)] with TOF for neutron energies below approximately 1 MeV [see Fig. 1(d)]. Prompt and random coincidences between neutrons and tritons, the latter corresponding to coincidences between particles from different beam bursts, were measured. The random events were subtracted from the prompt ones to give the true coincidences. The prompt-to-random ratio was 10:1 [see Fig. 1(c)].

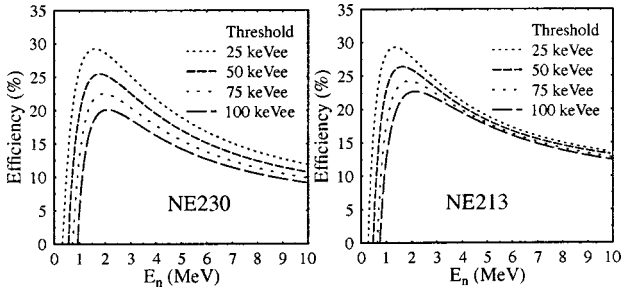

FIG. 2. Efficiency curves for thresholds between 25 keVee and 100 keVee for a NE230 detector (left) and a NE213 detector (right).

As the evaporation neutrons have a rather low energy (a Maxwellian-like distribution with the maximum close to 1 MeV), a very low threshold for the neutron detectors is needed to obtain an acceptable detection efficiency. In the experiment the thresholds were put as low as 30 keVee (which corresponds to approximately 350 keV neutron energy [13,33]). The energy calibration was done with the Compton edges of the 0.511 MeV and 1.275 MeV γ rays [34] from a ^{22}Na source and the full absorption peak of the 59.5 keV γ rays from a ^{241}Am source. The calibration and thresholds were verified in the course of the experiment.

Accurate knowledge of the thresholds is important in determining the efficiency curves for the detectors. For the NE230 detectors, efficiency measurements were available from an earlier similar experiment [13]. For the NE213 detectors, Monte Carlo simulations were performed using the code NEFF7 [35]. Typical efficiency curves, for a threshold ranging from 25 keVee to 100 keVee, are shown in Fig. 2 for both types of detectors. The efficiencies are used to correct the coincidence spectra for the neutron multiplicities. During the experiment lead foils of 2 mm thickness were placed in front of the detectors in order to reduce the counting rate due to γ rays.

Singles and coincidence data were taken simultaneously. The singles events were down-scaled by a factor of 10. Events due to singly ionized ^{3}He$^+$, where the beam particles pick up an electron in the target and thus end up in the focal plane with similar magnetic rigidity as the tritons [36], were to a large extent removed by putting a metal plate in between the two scintillators of the focal-plane detection system. Most ^{3}He particles were stopped in the metal plate, unlike the tritons. The small remainder of ^{3}He particles was used for energy and angle calibration, since its Q value and scattering angle are both zero. Further calibrations were performed using the ^{12}C(^{3}He,t) reaction and the ^{124}Sn(^{3}He,t) reaction itself, where the IAS is a convenient calibration. The

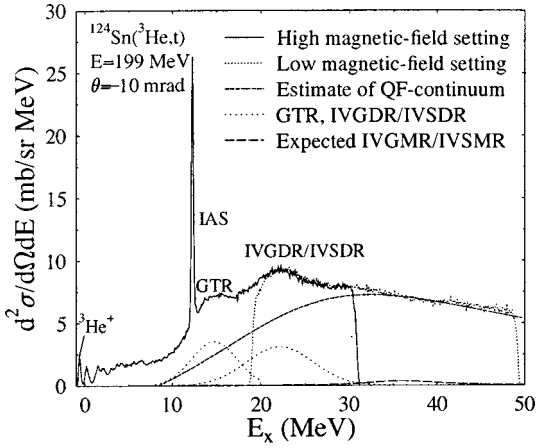

FIG. 3. Singles excitation-energy spectrum for the ^{124}Sn(^{3}He,t) reaction taken at $E(^3\mathrm{He})=199$ MeV and $\theta_t=-10$ mrad.

energy resolution was 300 keV [full width at half maximum (FWHM)] and the resolution in the horizontal scattering angle 2.6 mr. In the singles spectra some instrumental background due to reactions in the beam stop was present. Therefore, spectra obtained with an empty target frame were, after appropriate normalization, subtracted from the singles spectra. The beam stop was well shielded from the neutron detectors by the dipole magnet, and almost no instrumental background was present in the coincidence spectra.

The electronics live time was 99% and the focal-plane detection efficiency was approximately 85%, obtained by comparing accepted events to the trigger from the scintillator detectors. The XSYS data-acquisition system and graphical analysis package was used in the on-line and off-line analysis [37].

III. SINGLES DATA

In Fig. 3 the singles excitation-energy spectrum is shown for the low and high magnetic-field settings. The Q value for the reaction to the ground state of ^{124}Sb is -0.636 MeV. The small peak below $E_x=0$ MeV stems from singly ionized ^{3}He particles ($Q=0$). The large peak at an excitation energy of 12.2 MeV corresponds to the IAS. An estimate of the quasifree continuum is drawn in the figure based on the phenomenological description mentioned above. Estimates of the parameters used are very similar or equal to the ones used by Jänecke *et al.* [31] in the description of the quasifree continuum of the same reaction on ^{120}Sn.

Above 40 MeV this curve may slightly underestimate the data. This could be an indication for breakup-pickup contributions, which are expected to peak at a triton energy of 2/3 of the beam energy (i.e., at an ''apparent'' $E_x\approx 63$ MeV) with a width of 1/3 of the beam energy (65 MeV) [15,16].

The two curves with Lorentzian line shapes, centered at 14 MeV and 22 MeV, are results of a fit to the spectrum assuming the above-mentioned phenomenological description of the quasifree continuum. They correspond to the main component of the Gamow-Teller resonance (GTR) at 14 MeV and a combination of isovector giant dipole resonance (IVGDR, $\Delta L=1$, $\Delta S=0$, $\Delta T=1$) and spin-dipole resonance (IVSDR, $\Delta L=1$, $\Delta S=1$, $\Delta T=1$) at 22 MeV. IVSDR itself consists of three components with J^π equal to 0^-, 1^-, or 2^-. IVGDR and the three components of IVSDR cannot be distinguished since their relatively large widths make them overlap and their angular distributions are very similar because of the $\Delta L=1$ transfer.

Above an excitation energy of 25 MeV the spectrum is structureless. The excitation energy expected for IVGMR is calculated by [38]

$$E_X^{IVGMR}=E_X^{IAS}+V_0A^{-1/3}-(T_0+1)V_1/A, \tag{1}$$

where V_0 and V_1 depend on the model used, assuming that only the lowest of the three possible isospin components of IVGMR is excited. This is to a large extent true for heavy nuclei with a large neutron excess. For the reaction under consideration, more than 95% of the transition probability should go to this component as can be estimated from isospin-coupling (Clebsch-Gordan) coefficients. In the hydrodynamical model V_0 equals 170 MeV [38] but other approaches [21] suggest a lower value of 155 MeV. V_1 has been found to be strongly quenched with respect to the single-particle symmetry potential ($\approx$100 MeV [38]) and is approximately 60 MeV [19,21,39,40]. We thus find a rough estimate of 35 MeV for the excitation energy of VGMR in ^{124}Sb. For the width of IVGMR the situation is very unclear. Predictions vary between 5 and 25 MeV [1,19,21,41].

Calculations in the DWBA framework were performed to estimate the cross sections of IVGMR and IVSMR excited through the ^{124}Sn(^{3}He,t)^{124}Sb reaction. To this end, wave functions projected on a complete 1p-1h basis were calculated in a normal-mode procedure [38,42]. In this procedure, the responses of the nucleus to the action of an operator O is expanded over the 1p-1h basis:

$$|\mathrm{NM}_{T,LSJM}\rangle=N^{-1}\sum_{ph} v_{j_h}u_{j_p}|j_p,j_h^{-1};JM\rangle \times\langle j_pj_h^{-1};JM||O_{T,LSJ}||0\rangle. \tag{2}$$

For isovector non-spin-flip modes the operator is

$$O_{T=1,L0J}=r^\lambda Y_L t_z, \tag{3}$$

where λ usually equals the multipolarity L except for IVGMR in which case $\lambda=2$, and t_z is the isospin operator. For isovector spin-flip modes the operator is

$$O_{T=1,L1J}=r^\lambda[\sigma\otimes Y_L]_J t_z. \tag{4}$$

Similar to the non-spin-flip case, λ usually equals L, except for IVSMR in which case $\lambda=2$. Here, σ is the spin operator.

The fact that the last major neutron shell of ^{124}Sn is only partially filled was taken into account by using the experimentally determined neutron-hole occupation probabilities [fullness parameter $v^2(j)$] for this nucleus [43]. The proton-particle occupation probablities [emptiness parameter $u^2(j)$] for orbitals above the Fermi level are assumed to be 0 in the ground state of ^{124}Sn. Generally speaking, $v_j^2+u_j^2=1$ holds for all j.

TABLE I. Transition strengths calculated in a normal-mode procedure.

Mode	Strength
IAS	1.907[a]
IVGMR	755 fm^4
IVSMR	2266 fm^4

[a]Note that, when multiplied by 4π [because of the presence of Y_L with $L=0$ in the operator definition (3)], the value for the IAS equals 24, which is the Fermi sum rule $(N-Z)$ for ^{124}Sn.

The factor N in Eq. (2) is chosen such that the normal mode exhausts the full multipole strength:

$$S_{TLJ}=\sum_M |\langle \mathrm{NM}_{T,LSJM}|O_{T,LSJ}|0\rangle|^2$$

$$=\sum_{ph} v_{j_h}^2 u_{j_p}^2 |\langle j_p, j_h||O_{T,LSJ}||0\rangle|^2. \quad (5)$$

In other words, 100% of the non-energy-weighted sum rule (NEWSR) associated with the operator $O_{T,LSJ}$ is exhausted. For IVGMR and IVSMR, which are $2\hbar\omega$, $J^\pi=0^+$, and 1^+ transitions, respectively, many p-h configurations contribute. Calculations were performed using the code NORMOD [44]. The strengths calculated for IVGMR, IVSMR, and also the IAS are listed in Table I.

The value for IVGMR overestimates the result from the HF-RPA calculations by Auerbach and Klein [21] by 40%. [Note that the definition for the monopole operator used by the authors differs by a factor $\sqrt{8\pi}$ from Eq. (3). If this is taken into account, their number (1.1×10^4 fm^4) for IVGMR becomes 438 fm^4.] The reason for this overestimation is similar to the difference between HF-RPA and Tamm-Dancoff (TD) calculations [23], namely, that the HF-RPA approach takes ground-state correlations into account, in contrast to the TD and normal-mode calculations.

DWBA calculations were performed using the code DW81 [45]. An effective projectile-target interaction is used where the interaction is written in terms of Yukawa functions (for an extensive discussion see [25,46]). Parameters for the interaction were taken from the preliminary analysis of the ^{12,13,14}C(^{3}He,t)^{12,13,14}N reaction at 200 MeV [47] except for the central isospin strength (V_τ) which was determined from fitting the cross section of the IAS to the calculation. A value for V_τ of 3.46 ± 0.10 MeV was found, corresponding well to previously extracted values from (^{3}He,t) experiments at a similar bombarding energy [31,48]. The other parameters were taken, $V_{\sigma\tau}=-3.5$ MeV, $V_{T\tau}=-3.0$ MeV, while $V_{LS\tau}$ was kept zero [25]. The ^{3}He optical-model parameters were taken from the literature (^{3}He on ^{120}Sn at 217 MeV [49]). For the tritons the potential-well depths were taken 85% of the depths for the ^{3}He particles [50].

Results for transitions with $\Delta L=0$, 1, and 2 are displayed in Fig. 4. Besides IVGMR and IVSMR, at $E_x=35$ MeV (see above), these include the GTR ($E_x=13.25$ MeV), IVGDR ($E_x=22.0$ MeV), and IVSDR (components with $J^\pi=0^-$, 1^-, and 2^- at $E_x=23.8$ MeV, $E_x=22.9$ MeV, and $E_x=20.1$ MeV, respectively [51]), and isovector giant quadrupole resonance (IVGQR, $E_x=33.0$ MeV [52]). The appropriate normal-mode wave functions for each resonance were used. The monopole transitions peak at 0° and have a minimum around 3°. IVSMR is dominant over IVGMR by more than a factor of 3. Combined, the cross section of IVSMR and IVGMR at 0° is almost 70% of that for the IAS. A Lorentzian centered at an excitation energy of ~36 MeV, with a width (Γ) of 10 MeV and a cross section corresponding to this value, is drawn in Fig. 3. As can be seen, it only accounts for a small fraction of the total cross section contained in the continuum.

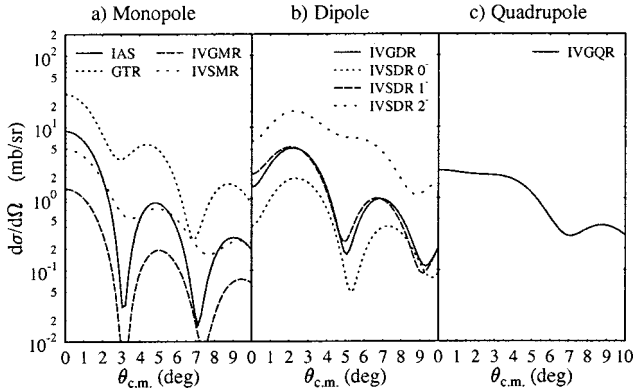

FIG. 4. Results of DWBA calculations for monopole (a), dipole (b), and quadrupole (c) resonances obtained using the normal-mode wave functions, i.e., exhausting the NEWSR for the respective giant resonances for ^{124}Sn(^{3}He,t) at $E(^3\mathrm{He})=199$ MeV.

Figure 4 further shows that the dipole resonances peak around 2.5°. The 2^- component of IVSDR is dominant. IVGQR is more or less flat below 4°. Its cross section at 0° being larger than that of the IVGMR but lower than that of IVSMR. It is expected at an excitation energy slightly lower than that of IVSMR and IVGMR [52], but since all these resonances have large widths, they should overlap.

The presence of monopole strength can be ascertained by comparing the excitation-energy spectra of particles with scattering angles around 0° and 2°. Since no vertical-angle information was available, the vertical angular slices around horizontal angles of 0° and 2° actually represent the centers of distributions of angles with $\Delta\Omega=0.715$ msr and $\Delta\Omega=0.525$ msr, respectively, i.e., only a fraction of the observed solid angle (4 msr), but with good angle definition. A completely independent analysis was performed, making use of the maximum possible solid angle, but reduced angle definition, with essentially identical results.

The result is shown in Fig. 5. In Fig. 5(c) the spectra taken at 0° (a) and 2° (b) are subtracted from each other. Resonances which have a maximum/minimum in the angular distribution at 0 ° will have positive/negative residuals. Contributions from the singly charged ^{3}He particles and from tritons due to the IAS and the GTR can be clearly distinguished. Between 2 and 10 MeV the weak positive excess in the difference spectrum stems from Gamow-Teller transitions corresponding to the theoretically predicted core-polarization and back-spin-flip strength (the so-called pygmy

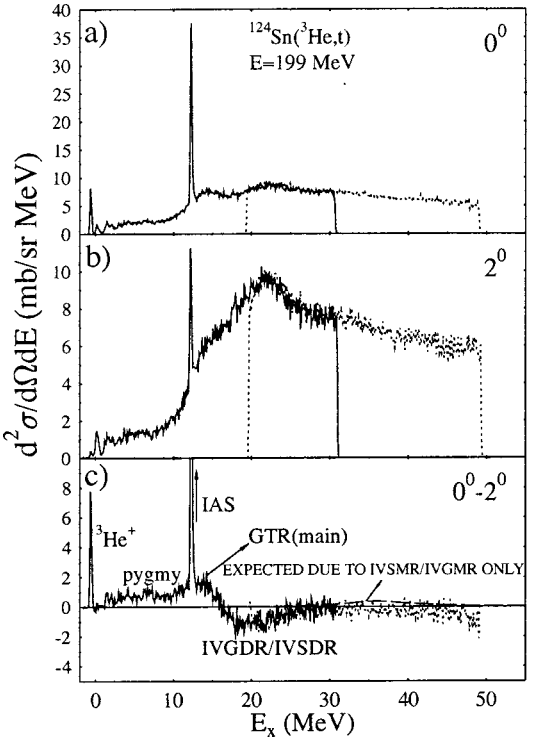

FIG. 5. Excitation-energy spectra for the ^{124}Sn(^{3}He,t) reaction at $\theta_t = 0°$ (a), $\theta_t = 2°$ (b), and their difference (c).

resonances [53]). They have been investigated for essentially all stable Sn isotopes [31,17]. The broad trough near the excitation energy of 21 MeV corresponds to dipole resonances. Above 27 MeV the difference spectrum is flat and consistent with zero. An estimate of the expected combined contribution from IVSMR and IVGMR to the difference spectrum is also included in Fig. 5(c), obtained by folding and subtracting the calculated cross sections in the DWBA for these resonances over the angular slices around horizontal scattering angles of 0° and 2° and assuming a Lorentzian line shape of width $\Gamma = 10$ MeV. It is clear from these singles data that there is no indication for the presence of monopole strength at high excitation energies.

IV. COINCIDENCE DATA

Figures 6(a) and 6(b) display the excitation-energy spectra gated on coincidences with neutrons and γ rays, respectively. Below an excitation energy of 6.5 MeV, decay by neutron emission is impossible because of the neutron-separation energy. When this channel opens the γ-ray emission drops to almost zero. A similar effect, although less strong, can be seen when the threshold for two-neutron emission is reached at $E_x = 15.5$ MeV. Thresholds for the emission of three, four, five, and six neutrons lie at 22.3 MeV, 31.5 MeV, 38.5 MeV, and 48.1 MeV, respectively (also indicated in the figure), but at higher excitation energies the steps in the spectra get less distinct because of a convolution over the phase spaces for multiple consecutive neutron emission.

Events where at least one neutron was detected in coincidence with a triton were accepted for the spectrum of Fig. 6(a). Therefore, the spectrum is biased with regard to neutron multiplicity. This has to be taken into account in order to obtain corrected neutron-gated triton-energy spectra. This correction is furthermore complicated by the fact that the efficiency is energy dependent as described above.

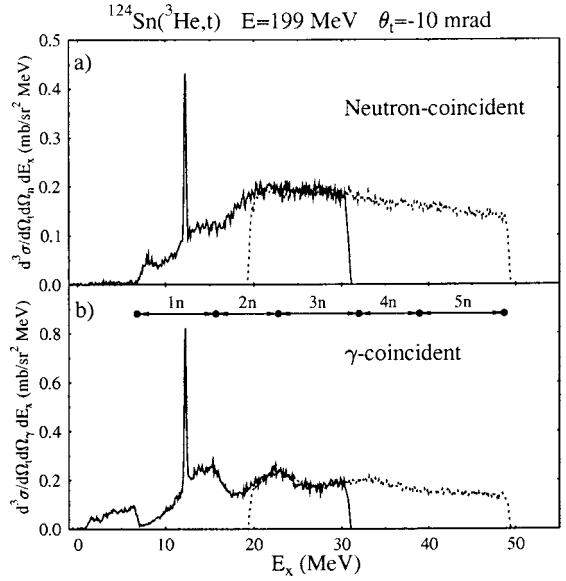

FIG. 6. Neutron (a) and γ-ray (b) coincidence spectra for the ^{124}Sn(^{3}He,t) reaction. The thresholds for decay by neutron emission are also indicated.

To determine the multiplicity as a function of excitation energy, statistical-model calculations were performed in the Hauser-Feshbach formalism [54], using the computer code CASCADE [55]. The decay probabilities for decays from excited states in the nucleus ^{124}Sb into the various channels are calculated using the statistical weights of the final states and the barrier penetrabilities. It is assumed that the excited nucleus has reached full statistical equilibrium and (semi)direct decay is thus neglected.

Major inputs into the calculations are the level densities for the nuclei involved in the decay cascade. For this purpose, the total range of excitation energy for each nucleus involved has been divided into four regions. In the first region experimentally known levels (n_1) up to an energy E_1 (see Table II) are used to calculate the level density [56]. In the second region, up to 12 MeV (E_2), the backshifted Fermi-gas model [57] is used to estimate the level densities. In Table II, the corresponding level-density parameter a_2 [level density = mass(A)/a_2] and backshift pairing-energy parameter Δ_2 [58] are given. In the fourth region above 25 MeV (E_3), the level density is calculated based on a liquid-drop model, and the values for the same parameters as used in the second region are again listed in the table [59]. In the excitation-energy range between regions 2 and 4, level densities are smoothly interpolated.

The result of the statistical-model calculation for the neutron-emission spectrum from a certain excitation energy is a Maxwellian-like distribution. The distribution displayed in Fig. 7(a) is for $E_x = 30$ MeV. The integral of this distribution gives the multiplicity. In the same figure, the conse-

TABLE II. Level-density parameters used in CASCADE calculations.

Nucleus	Region 1		Region 2			Region 4		
	E_1 (MeV)	n_1	E_2 (MeV)	a_2 (MeV^{-1})	Δ_2 (MeV)	E_3 (MeV)	a_4 (MeV^{-1})	Δ_4 (MeV)
^{124}Sb	0.40	17	12.0	8.83	-1.39	25.0	8	-3.91
^{123}Sb[a]	1.10	5	12.0	8.40	-1.30	25.0	8	-3.13
^{122}Sb	0.48	26	12.0	8.18	-1.21	25.0	8	-4.30
^{121}Sb[a]	1.33	10	12.0	8.06	-1.12	25.0	8	-3.44
^{120}Sb[a]	0.45	17	12.0	8.00	-1.03	25.0	8	-4.56
^{119}Sb[a]	1.68	22	12.0	7.93	0.	25.0	8	-3.72
^{123}Sn	1.12	15	12.0	8.82	0.970	25.0	8	-2.43
^{122}Sn[a]	2.80	20	12.0	8.72	1.210	25.0	8	-1.59

[a] a_2 and Δ_2 are interpolated values.

quence of folding with the detection efficiency is also shown for thresholds ranging between 25 and 100 keV *ee* (for the NE230 scintillator). As one can see, the multiplicity that would be measured decreases strongly with increasing *n*-detection threshold. In Fig. 7(b) this effect is shown for excitation energies in ^{124}Sb up to 50 MeV. Also, the steps clearly visible in the uncorrected CASCADE calculations, Fig. 7(b), become increasingly less pronounced when corrected for detection efficiency.

The efficiency-corrected multiplicity curves were calculated separately for each detector and for the low- and high-magnetic-field settings, because the detection thresholds shifted between these measurements. For each detector the experimentally determined coincidence spectra were then divided by the corresponding calculated curve. Finally, the corrected spectra from all detectors were added. The result is shown in Fig. 8.

A branching ratio of 89 ± 2 % for the decay by neutron emission from the IAS was extracted from the data. Here, the error is statistical only. This value is in agreement with the predicted value of 91.1 ± 5.1 % [32]. For the range from 10 to 16 MeV, including the IAS, a branching ratio of ~90% is found. This result indicates that the GTR also strongly decays by neutron emission. Decay from the dipole resonances was also observed.

Surprisingly, a large nonresonant component is still present in the neutron-gated coincidence spectrum, even at high excitation energies. Above 30 MeV the coincidence cross section still accounts for ~50% of the singles cross section. This was determined by assuming isotropy of neutron emission. Therefore, the expected contribution from the monopole resonances, again indicated by a Lorentzian, is still small compared to the observed neutron-gated cross section. The estimate for IVSMR and IVGMR was drawn under the assumption that the branching ratio for decay by neutron emission is the same as for the IAS.

Again, it was attempted to enhance the possible presence of monopole strength by comparing spectra from small and large scattering angles. The coincidence spectra taken at 0° and 2° are shown in Fig. 9. A binning of 1 MeV has been chosen. These coincidence spectra correspond to the singles spectra of Figs. 5(a) and 5(b). In Fig. 10(a), the difference spectrum is displayed. An estimate of the expected IVGMR and IVSMR monopole strength is again included, following

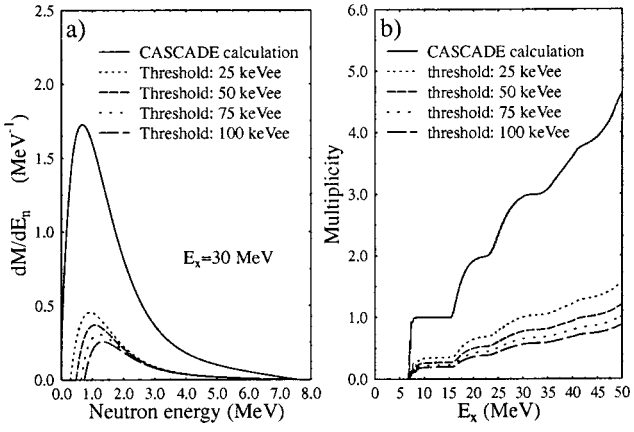

FIG. 7. Energy distribution of emitted neutrons from an excitation energy of 30 MeV (a) as calculated using the computer code CASCADE. The effect of a change in detection threshold is indicated by the various curves. Neutron-multiplicity versus excitation-energy curves (b). Again the influence of the detection threshold is indicated.

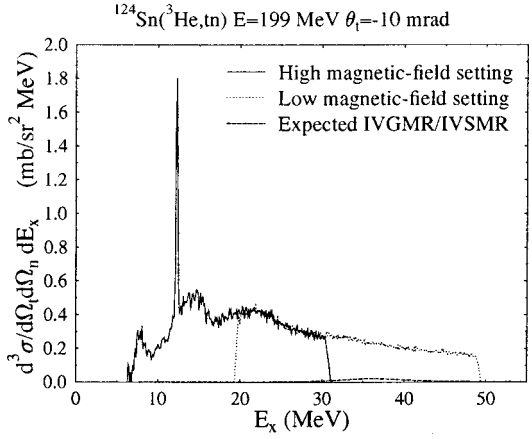

FIG. 8. Excitation-energy spectrum measured in coincidence with neutrons, corrected for neutron-detection efficiency and multiplicity. An estimate for IVGMR and IVSMR is shown with a Lorentzian line shape.

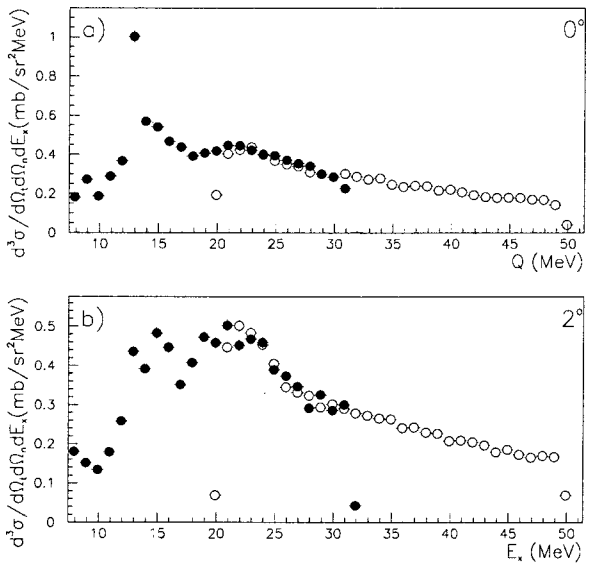

FIG. 9. Corrected neutron-coincident excitation-energy spectra obtained at (a) $\theta_t = 0°$ and (b) $\theta_t = 2°$. Solid and open circles are from the high- and low-magnetic-field runs, respectively.

the same procedure as for the singles data and assuming an equal branching ratio for decay by neutron emission from IVGMR and IVSMR as for the IAS. The error bars are statistical only. The IAS, GTR, and dipole resonances are clearly visible. There is no indication for monopole strength at higher excitation energies, not even with an increased bin size of 4 MeV [Fig. 10(b)] to account for the increased linewidth or fragmentation. The data are clearly consistent with zero. Under the assumptions that contributions with multipolarities larger than zero do not contribute to the difference

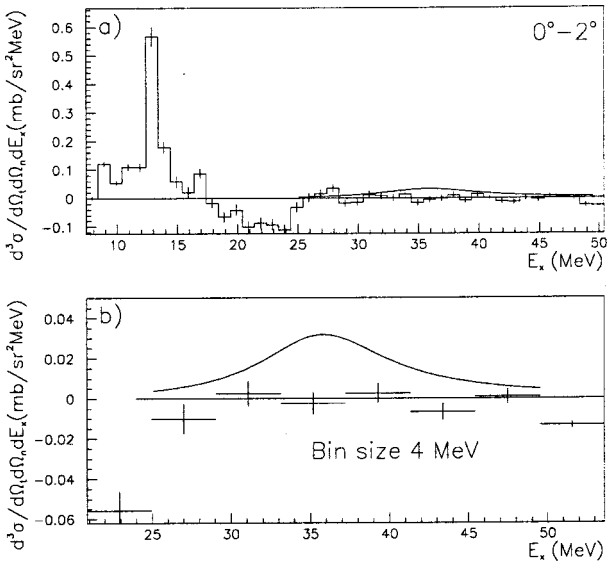

FIG. 10. (a) The difference spectrum obtained by subtracting spectra of Figs. 9(a) and 9(b). (b) is similar to (a) but for the high-excitation-energy range only and with a binning of 4 MeV. Estimates for IVGMR and IVSMR are shown with Lorentzian line shapes.

spectrum at high excitation energies and that the isovector monopole resonances are Lorentzian distributed as indicated in the figures, it can be calculated that with a certainty of 95% the cross section for the isovector monopole resonances is below 20% of the expected cross section on the basis of DWBA calculations with normal-mode wave functions.

V. INTERPRETATION AND CONCLUSIONS

A major conclusion from the present work is the failure to observe monopole strength at high excitation energies. This result is in part due to the presence of a nonresonant continuum background. While such a background is known to exist in singles mode, the presence of still significant contributions from events gated on coincidences with neutrons was unexpected. Furthermore, the problems in the ray-tracing procedure for the vertical direction made the difference-of-spectra method less sensitive than it could have been. Nevertheless, estimates for the expected monopole strength exceed the data beyond their statistical uncertainties in both singles and coincidence modes, but particularly for the latter.

This result may be due to an overestimate of the expected monopole strength. The Lorentzian curves shown in Figs. 5(c), 10(a), and 10(b) are estimates for the combined cross section of IVGMR and IVSMR and were calculated under the assumption that the widths of these resonances (Γ) are 10 MeV. If the widths are much larger, as suggested by Auerbach and Klein [21,23] and by results from π-charge-exchange [1] data, finding the strength would become increasingly difficult. Also, the monopole cross sections decrease strongly with increasing momentum transfer and thus increasing Q value. Therefore, if the resonances are centered around a higher excitation energy than the values assumed here (36 MeV), the estimates drawn in this paper are too high. Performing the strength calculations for IVGMR and IVSMR in the framework of normal modes, as was done in the present work, might lead to an overestimation of the strengths (up to 40% with respect to HF-RPA calculations) and thus the cross section.

Furthermore, the assumption that the branching ratios for statistical decay by neutron emission from IVSMR and IVGMR are similar to that from the IAS could be wrong. It can be argued that the Coulomb barrier is relatively less important than at lower excitation energies and thus direct decay by proton emission becomes more likely.

The large cross section measured for the continuum at high excitation energies in coincidence with neutrons in the backward direction, essentially 50% of the singles cross section (assuming isotropic decay), is not understood. It appears that there are several possible explanations. First, the quasifree knock-on charge-exchange and breakup-pickup processes, discussed earlier, could lead to neutron emission. Second, other processes may result in the emission of neutrons. Finally, considerations related to the data reduction may affect the results (see below).

The quasifree processes are believed to lead to single-neutron-hole states in the nucleus ^{123}Sn at excitation energies predominantly below the threshold for neutron emission. This was the primary argument for performing the

experiment described here. The final nucleus would, therefore, not emit neutrons and the quasifree nonresonant background at higher excitation energies could therefore be suppressed or at least reduced considerably using coincidence measurements. However, it was also known that a presumably small fraction will excite deep-hole states. Therefore, the remaining nucleus could be in a rather highly excited neutron-hole state and thus decay statistically by neutron emission. However, a strong excitation of these deep-hole states relative to valence-shell excitations is very unlikely. It must also be noted that if statistical decay happens from a nucleus excited in a quasifree process, it cannot be deduced from the singles measurements or coincidence measurements with neutrons detected at backward angles what the excitation energy of such a nucleus is. This influences the multiplicity calculations. Also, more complicated, two- or more-step processes that result in the emission of neutrons at backward angles could be more important than expected.

If the high-excitation-energy region also contains contributions from other broad resonances (other than IVGMR and IVSMR), these can decay by neutron emission and account for part of the measured coincidence cross section at backward angles. To investigate this, one has to calculate strength distributions and differential cross sections for such resonances. This has not been attempted in the present work.

The efficiency and multiplicity corrections may give rise to systematic errors. It is estimated that the determination of the neutron detection threshold could be off by 10 keV*ee*. For an excitation energy of 30 MeV [the example shown in Fig. 7(a)] this changes the efficiency-corrected multiplicity by approximately 10%. This can only be circumvented by measuring neutron energies (TOF), thereby losing solid angle. An error in the correction procedure can, however, not explain the failure in finding monopole strength at higher excitation energies, since a cross section that is consistent with zero in the difference spectrum will remain zero, even if the correction changes.

It is implausible that the above conjectures can explain the observed strong cross section in the continuum region at high excitation energies for events gated on coincidences with neutrons in the backward direction. Therefore, it is concluded that, contrary to expectations, there is still a significant probability for emission of neutrons (50% if isotropic emission is assumed) of unknown origin. This makes the observation of the expected broad isovector spin-flip and non-spin-flip resonances in this region of excitation energies in coincidence experiments with neutrons difficult.

ACKNOWLEDGMENTS

The authors wish to thank the cyclotron crew and technical staff at IUCF for their support. The research was supported by the U.S. National Science Foundation and is part of the research program of the Dutch ''Stichting voor Fundamenteel Onderzoek der Materie'' (FOM) with financial support from the ''Nederlandse Organisatie voor Wetenschappelijk Onderzoek'' (NWO). Support by the Scientific Affairs Division of the North Atlantic Treaty Organization (NATO), Research Grant No. 900 219, and the Office of the Vice-President for Research, University of Michigan, is gratefully acknowledged.

[1] A. Erell, J. Alster, J. Lichtenstadt, M. A. Moinester, J. D. Bowman, M. D. Cooper, F. Irom, H. S. Matis, E. Piasetzky, and U. Sennhauser, Phys. Rev. C **34**, 1822 (1986).

[2] A. Erell, J. Alster, J. Lichtenstadt, M. A. Moinester, J. D. Bowman, M. D. Cooper, F. Irom, H. S. Matis, E. Piasetzky, U. Sennhauser, and A. Ingram, Phys. Rev. Lett. **52**, 2134 (1984).

[3] F. Irom, J. D. Bowman, G. O. Bolme, E. Piasetzky, U. Sennhauser, J. Alster, J. Lichtenstadt, M. A. Moinester, J. N. Knudson, S. H. Rokni, and E. R. Siciliano, Phys. Rev. C **34**, 2231 (1986).

[4] S. Nakayama, H. Akimune, Y. Arimoto, I. Daito, H. Fujimura, Y. Fujita, M. Fujiwara, K. Fushimi, H. Kohri, N. Koori, K. Takahisa, T. Takeuchi, A. Tamii, M. Tanaka, T. Yamagata, Y. Yamamoto, K. Yonehara, and H. Yoshida, Phys. Rev. Lett. **83**, 690 (1999).

[5] T. D. Ford, J. L. Romero, F. P. Brady, C. M. Castaneda, J. R. Drummond, B. McEachern, D. S. Sorensen, Zin Aung, N. S. P. King, A. Klein, and W. G. Love, Phys. Lett. B **195**, 311 (1987).

[6] C. Bérat, M. Buénerd, J. Y. Hostachy, P. Martin, J. Barrette, B. Berthier, B. Fernandez, A. Miczaïka, A. Villari, H. G. Bohlen, S. Kubono, E. Stiliaris, and W. von Oertzen, Nucl. Phys. **A555**, 455 (1993).

[7] I. Lhenry, Nucl. Phys. **A599**, 245c (1996).

[8] W. von Oertzen, Nucl. Phys. **A482**, 357c (1988).

[9] C. Ellegaard, C. Gaarde, J. S. Larsen, C. Goodman, I. Bergqvist, L. Carlén, P. Ekström, B. Jakobsson, J. Lyttkens, M. Bedjidian, M. Chamcham, J. Y. Grossiord, A. Guichard, M. Gusakow, R. Haroutunian, J. R. Pizzi, D. Bachelier, J. L. Boyard, T. Hennino, J. C. Jourdain, M. Roy-Stephan, M. Boivin, and P. Radvanyi, Phys. Rev. Lett. **50**, 1745 (1983).

[10] N. Auerbach, F. Osterfeld, and T. Udagawa, Phys. Lett. B **219**, 184 (1989).

[11] D. L. Prout *et al.*, in *Polarization Phenomena in Nuclear Physics*, edited by E. J. Stephenson and S. Vigdor, AIP Conf. Proc. 339 (AIP, New York, 1995), p. 458.

[12] J. A. Bordewijk, A. Balanda, D. Beaumel, J. Blomgren, S. Brandenburg, G. van 't Hof, M. N. Harakeh, M. A. Hofstee, J. Jänecke, A. Krasznahorkay, H. Laurent, L. Nilsson, N. Olsson, R. Perrino, R. Siebelink, P. O. Söderman, S. Y. van der Werf, and A. van der Woude, Nucl. Phys. **A574**, 453 (1994).

[13] D. A. Roberts, K. Ashktorab, F. D. Becchetti, J. Jänecke, M. N. Harakeh, S. Y. van der Werf, G. P. A. Berg, C. C. Foster, J. E. Lisantti, T. Rinckel, E. J. Stephenson, S. P. Wells, A. Nadasen, and S. Shaheen, Phys. Rev. C **52**, 1361 (1995).

[14] E. H. L. Aarts, R. K. Bhowmik, R. J. de Meijer, and S. Y. van der Werf, Phys. Lett. **102B**, 307 (1981).

[15] O. Bousshid, H. Machner, C. Alderliesten, U. Bechstedt, A. Djaloeis, P. Jahn, and C. Mayer-Böricke, Phys. Rev. Lett. **45**, 980 (1980).

[16] S. Gopal, A. Djaloeis, J. Bojowald, O. Bousshid, W. Oelert, N. G. Puttaswamy, P. Turek, and C. Mayer-Böricke, Phys. Rev. C **23**, 2459 (1981).
[17] K. Pham, J. Jänecke, D. A. Roberts, M. N. Harakeh, G. P. A. Berg, S. Chang, J. Liu, E. J. Stephenson, B. F. Davis, H. Akimune, and M. Fujiwara, Phys. Rev. C **51**, 526 (1995).
[18] N. Auerbach, Nucl. Phys. **A182**, 247 (1972).
[19] N. Auerbach and A. Yeverechyahu, Ann. Phys. (N.Y.) **95**, 35 (1975).
[20] N. Auerbach and A. Klein, Phys. Rev. C **28**, 2075 (1983).
[21] N. Auerbach and A. Klein, Nucl. Phys. **A395**, 77 (1983).
[22] S. Adachi and N. Auerbach, Phys. Lett. **131B**, 11 (1983).
[23] N. Auerbach and A. Klein, Phys. Rev. C **30**, 1032 (1984).
[24] W. G. Love and M. A. Franey, Phys. Rev. C **24**, 1073 (1981).
[25] F. Osterfeld, Rev. Mod. Phys. **64**, 491 (1992).
[26] N. Auerbach, Comments Nucl. Part. Phys. **22**, 223 (1998).
[27] G. P. A. Berg, L. C. Bland, D. Duplantis, C. C. Foster, D. W. Miller, P. Schwandt, R. Sawafta, K. Solberg, and E. J. Stephenson, IUCF Annual Report 1988, p. 223.
[28] G. P. A. Berg, S. Wells, Y. Wang, T. Hall, A. Bacher, D. Bilodeau, J. Doskow, G. East, C. C. Foster, J. Lisantti, T. Rinckel, P. Schwandt, and E. J. Stephenson, IUCF Annual Report 1991, p. 221.
[29] G. P. A. Berg, C. C. Foster, E. J. Stephenson, and B. F. Davis, IUCF Annual Report 1994, p. 106.
[30] J. Jänecke, F. D. Becchetti, A. M. van den Berg, G. P. A. Berg, G. Brower, M. B. Greenfield, M. N. Harakeh, M. A. Hofstee, A. Nadasen, D. A. Roberts, R. Sawafta, J. M. Schippers, E. J. Stephenson, D. P. Stewart, and S. Y. van der Werf, Nucl. Phys. **A526**, 1 (1991).
[31] J. Jänecke, K. Pham, D. A. Roberts, D. Stewart, M. N. Harakeh, G. P. A. Berg, C. C. Foster, J. E. Lisantti, R. Sawafta, E. J. Stephenson, A. M. van den Berg, S. Y. van der Werf, S. E. Muraviev, and M. H. Urin, Phys. Rev. C **48**, 2828 (1993).
[32] J. Jänecke, J. Bordewijk, M. N. Harakeh, and S. Y. van der Werf, Nucl. Phys. **A552**, 323 (1993).
[33] D. L. Smith, R. G. Polk, and T. G. Miller, Nucl. Instrum. Methods **64**, 157 (1968).
[34] G. Dietze and H. Klein, Nucl. Instrum. Methods Phys. Res. **193**, 549 (1982).
[35] G. Dietze and H. Klein, computer codes NRESP4 and NEFF4, Physikalisch-Technische Bundesanstalt ND22, 1982. Updated versions NRESP7 and NEFF7, 1991 (unpublished).
[36] K. Dennis, H. Akimune, G. P. A. Berg, S. Chang, B. Davis, M. Fujiwara, M. N. Harakeh, J. Jänecke, J. Liu, K. Pham, D. A. Roberts, and E. J. Stephenson, Phys. Rev. A **50**, 3992 (1994).
[37] N. Yoder, IUCF data-acquisition software, IUCF Technical Report, 1998; K600 routines by E. J. Stephenson, IUCF; neutron-detection routines by D. A. Roberts, University of Michigan.
[38] A. Bohr and B. R. Mottelson, *Nuclear Structure* (Benjamin, New York, 1975), Vols. 1 and 2.
[39] R. Ö. Akyüz and S. Fallieros, Phys. Rev. Lett. **27**, 1016 (1971).
[40] P. Paul, F. Amann, and K. A. Snover, Phys. Rev. Lett. **27**, 1013 (1971).
[41] J. Jänecke, M. N. Harakeh, and S. Y. van der Werf, Nucl. Phys. **A463**, 571 (1987).
[42] M. A. Hofstee *et al.*, Nucl. Phys. **A588**, 729 (1995).
[43] E. J. Schneid, A. Prakash, and B. L. Cohen, Phys. Rev. **156**, 1316 (1967).
[44] S. Y. van der Werf, computer code NORMOD (unpublished).
[45] R. Schaeffer and J. Raynal, computer code DWBA70, 1970 (unpublished); extended version DW81 by J. R. Comfort, 1981 (unpublished).
[46] S. Y. van der Werf, Phys. Scr. **T32**, 43 (1990).
[47] J. Jänecke *et al.* (unpublished).
[48] R. G. T. Zegers, Ph.D. thesis, Rijksuniversiteit Groningen, 1999.
[49] N. Willis, I. Brissaud, Y. le Bornec, B. Tatischeff, and G. Duhamel, Nucl. Phys. **A204**, 454 (1973).
[50] S. Y. van der Werf, S. Brandenburg, P. Grasdijk, W. A. Sterrenburg, M. N. Harakeh, M. B. Greenfield, B. A. Brown, and M. Fujiwara, Nucl. Phys. **A496**, 305 (1989).
[51] V. A. Kuzmin and V. G. Soloviev, J. Phys. G **11**, 603 (1985).
[52] See, for example, *Electric and Magnetic Giant Resonances in Nuclei*, edited by J. Speth, International Review of Nuclear Physics, Vol. 7 (World Scientific, Singapore, 1991).
[53] Y. V. Gaponov and Y. S. Lyutostanskii, Sov. J. Nucl. Phys. **19**, 33 (1974).
[54] W. Hauser and H. Feshbach, Phys. Rev. **87**, 366 (1952).
[55] F. Pühlhofer, Nucl. Phys. **A280**, 267 (1977); Computer code CASCADE, 1979 (unpublished); M. N. Harakeh, extended version.
[56] R. R. Kinsey, Nuclear Data Sheets v2.5, National Nuclear Data Center, Brookhaven National Laboratory, Internet BNLND2.DNE.BNL.GOV, 1996.
[57] E. Gadioli and R. Zetta, Phys. Rev. **167**, 1016 (1968).
[58] W. Dilg, W. Schantl, H. Vonach, and M. Uhl, Nucl. Phys. **A217**, 269 (1973).
[59] W. D. Myers, *Droplet Models of Atomic Nuclei* (Plenum, New York, 1977).